J Mater Sci (2010) 45:4796–4804
DOI 10.1007/s10853-010-4600-7

ULTRAFINE GRAINED MATERIALS

Tensile and compressive test in nanocrystalline and ultrafine carbon steel

R. Rodríguez-Baracaldo · J. A. Benito · J. M. Cabrera

Received: 13 February 2010 / Accepted: 4 May 2010 / Published online: 19 May 2010

Abstract Plastic deformation behavior was investigated in near fully dense nanostructured and ultrafine-grained bulk samples of carbon steel (0.55 wt% C) under compression and tension tests. The specimens were obtained by hot pressure from mechanically milled powder at 400 and 500 °C. Subsequent heat treatments at temperatures going from 600 to 900 °C produced samples with ferrite grain sizes from 30 nm to 17 μm. Nanocrystalline grained steel samples presented very high strength with low ductility. Once, in the ultrafine range, as the ferritic grain size was increased, the strength was decreased and the ductility was improved. The porosity and carbon atoms within the structure were analyzed in order to explain the results of strength and strain obtained.

R. Rodríguez-Baracaldo (✉)
Department of Industrial Engineering, Universidad Nacional de Colombia, Campus La Nubia, Manizales, Colombia
e-mail: rrodriguezba@unal.edu.co

J. A. Benito
Department of Materials Science and Metallurgical Engineering, EUETIB, Universitat Politècnica de Catalunya, Comte d'Urgell 187, 08036 Barcelona, Spain

J. M. Cabrera
Department of Materials Science and Metallurgical Engineering, ETSEIB, Universitat Politècnica de Catalunya, Av. Diagonal 647, 08028 Barcelona, Spain

J. A. Benito · J. M. Cabrera
Centre Tecnològic CTM, Av. Bases de Manresa 1, 08240 Manresa, Spain

Introduction

Grain refinement is an important strengthening mechanism for steels. Ultrafine-grained materials (UFG) with grain sizes above 100 nm but within the nanometric range and nanocrystalline materials (NC) with grain sizes below 100 nm exhibit an enhanced mechanical strength [1–4]. The main benefits are the prevention of alloying elements and heat treatments. NC/UFG steels have great potential for replacing some conventional high-strength steels. However, the ductility is drastically reduced in NC/UFG steels comparing them to their coarse-grained counterparts. The uniform elongation of these steels before inhomogeneous or localized deformation is much lower than steels with a larger grain size. In recent years, there has been an increase in research to improve the ductility that might be achieved in NC/UFG materials through the use of various procedures such as a bi-modal grain size distribution, nanotwins, boundary structure engineering, and second phase precipitation. However, these approaches decrease in strength as they increase in ductility [5–8].

According to Considere criteria, a large hardening capability is required to show uniform deformation for metals with high strength; such as NC/UFG steel [9]. The great majority of reported NC/UFG iron and steel show few or none hardening capability and even some papers reported softening due to formation of shear bands as dominant deformation mechanism [10–15]. Several authors have studied microstructure and mechanical behavior of NC/UFG structure of mechanically milled iron and steel. Mechanical characterization on iron powder without a consolidation process was carried out by numerous authors [16–20]. Others works carried out mechanical tests on bulk samples, for example: specimens obtained by hot rolling of powder previously encapsulated in steel tubes [21–23],

samples obtained by hot uniaxial pressing [12, 24], by hot isostatic pressing [25], and by hot extrusion [26]. Each work reported different results as a function of obtaining and characterization methods used. Studies of NC iron powder with oxygen intentionally added have shown an increase of strength due to the presence of nanosized oxide particles. [27–29]. High mechanical properties are worth noting in NC steel obtained by dynamic impact [30], and ball drop [31, 32]. Iron samples obtained by spark plasma sintering [33–35] displayed a high strength and decent ductility.

NC/UFG steels can be obtained through different processing routes, such as powder metallurgy techniques, severe plastic deformation, and thermomechanical treatments. Powder metallurgy technique has been widely used due to its simplicity and low cost. During mechanical milling occurs the grain refinement exhibiting a strong increasing of mechanical properties and changing thermal and magnetic properties that depend on the nanometric structure obtained [19]. Powder with very small grain size (20 nm) is consolidated into bulk samples completing the powder metallurgy technique. Nevertheless, contamination, imperfect particle bonding, and volume flaws are some problems associated with this procedure [36, 37]. On the other hand, steels obtained by severe plastic deformation process are treated as solid materials without the problems of the porosity of powder metallurgy. Grain size reduction reached by these processes is normally larger than 300 nm though. Specimens through equal channel angular pressing (ECAP) [38, 39] and accumulative rolling bonding (ARB) [40–43] were studied by tensile test showing acceptable ductility.

Compressive and tensile deformation behavior is an interesting subject of study since a difference is often observed between them. However, the comparison from samples produced with different methods often show inconsistent results. The aim of this work is to analyze the compressive and tensile behavior of NC/UFG bulk specimens of 0.55 wt% C steels obtained by hot consolidation process of mechanical milled steel powder. Samples with a wide range of grain size were used to correlate the deformation behavior with the grain size. The determination of mechanical properties by compressive and tensile test developed in this work can make a contribution to understand the ductility problems of these materials.

Materials and method

A commercial pure iron powder was severely deformed in a planetary ball mill with stainless steel balls under an Ar gas atmosphere. The medium carbon steel samples were obtained by milling the powder with a small amount (0.8 wt%) of Etilen-bis-stearamide (EBS) for 52 h. The addition of EBS also avoided the adherence of the powder to the recipient walls. The final chemical composition (wt%) was 0.55 C, 0.73 O, 0.27 Cr, 0.15 Ni, and Fe balance. The consolidation process of the steel powders was divided into two steps. In the first one, the powder was cold compacted at 1100 MPa for 30 min. The second step was a hot uniaxial compaction at a fixed pressure of 850 MPa for 60 min. The hot compaction temperatures chosen were between 425 and 500 °C, in order to obtain different grain sizes inside the nanocrystalline and low ultrafine regimes. Some as-consolidated specimens at 500 °C were additionally heat treated at temperatures between 600 and 900 °C during 30 min in a tubular furnace under an Ar protective atmosphere and subsequently cooled down in an Ar atmosphere in order to get different grain sizes.

The dimensions of the cylindrical specimens used in the compression tests were 5 mm in length and 7 mm in diameter. Specimens for tensile test were cut from consolidated samples of 1 mm in length and 10 mm in diameter by using a wire electrical discharge machine. The tensile tests were carried out with samples dimensions outside the standard procedure due to the geometric limitations. The samples were 1 mm wide, 0.8–1 mm thick, and 2 mm of gage length. The density was determined first by measuring the dimensions and weight of the consolidated samples and secondly by the Archimedes method. The total porosity determined by both methods was lower than 4% in all the examined samples. Porosity was also observed in the internal longitudinal section of the specimens by scanning electron microscopy (SEM) after four cycles consisting of etching with Nital 2% and polishing cloth.

The ferritic grain sizes of steel samples obtained under different treatments were determined by SEM and transmission electron microscopy (TEM). Samples for TEM observation were elaborated by ion milling. The grain size in the nanocrystalline samples was measured combining bright and dark field TEM images. This procedure allowed identifying the contour of grains free from overlapping effects. For the heat treated samples at temperatures above 725 °C in which larger amount of cementite precipitates were formed, the microstructures were also observed in the transverse directions of the cylinders by SEM after etching the specimens with Nital 2%. Compression tests on bulk specimens were performed on a universal testing machine at a strain rate of $1 \cdot 10^{-4}$ s^{-1}, and Teflon sheet and lithium grease were applied in order to minimize friction. Tensile tests were conducted in a Deben tensile machine at an initial strain rate of $1.7 \cdot 10^{-3}$ s^{-1}. Lateral surfaces of tensile samples were ground, polished, and analyzed by SEM in order to identify shear bands or any deformation sign.

Results and discussion

Microstructural characterization

The average grain size of the ferrite for the different as-consolidated samples is shown in Table 1 together with the corresponding values of relative density and total area porosity. Also the evolution of the microstructure with the processing temperature can be observed in the TEM micrographs shown in Fig. 1.

In general terms, when the consolidation temperature increases, a slight growth of the average ferrite grain size is produced, while the random orientation of the nanocrystalline grains of ferrite remains. Nanocrystalline ferrite grains are visible but their grain boundaries are not clearly distinguishable, which raised some difficulties in the determination of the ferritic grain size by TEM. The lowest temperature used in the consolidation process (425 °C) creates samples with an average grain size of ~30 nm. The continuous rings in select diffraction area (SAD) confirm a

Table 1 Consolidation procedure, grain size and porosity values of the consolidated samples

Consolidation procedure	Grain size (nm)	Relative density (%)	Total area porosity (%)
HC 425 °C	30 ± 19	>96	2.15
HC 460 °C	46 ± 21	>96	1.69
HC 500 °C	115 ± 45	>97	1.38
HC 500 °C + HT 650 °C	160 ± 40	>97	1.23
HC 500 °C + HT 700 °C	340 ± 220	>97	1.25
HC 500 °C + HT 725 °C	390 ± 180	>97	1.21
HC 500 °C + HT 775 °C	900	>97	1.22
HC 500 °C + HT 825 °C	1100	>97	1.12
HC 500 °C + HT 875 °C	2800	>97	1.14
HC 500 °C + HT 1100°C	17000	>98	1.03

HC hot compaction temperature, *HT* heat treatment

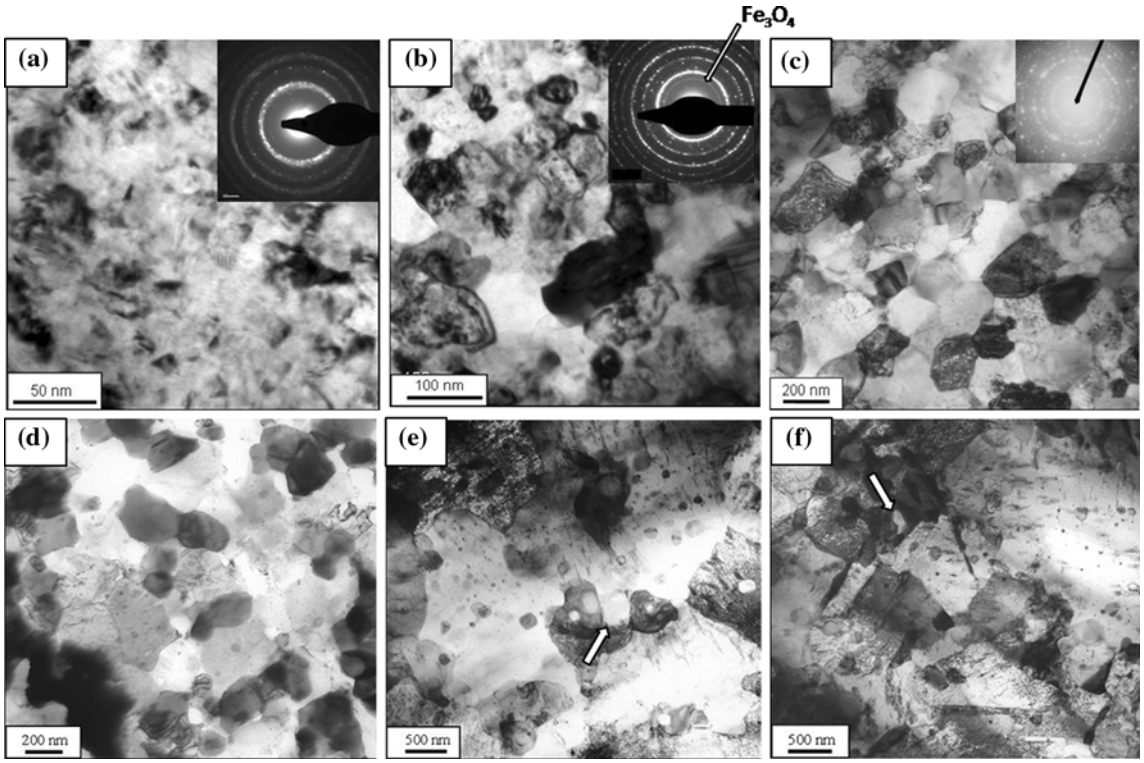

Fig. 1 TEM images for different consolidation procedures. **a** HC 425 °C, **b** HC 460 °C, **c** HC 500 °C, **d** HC 500 °C + HT 725 °C, **e** HC 500 °C + HT 775 °C, **f** HC 500 °C + HT 825 °C. The rings marked in the selected diffraction area confirm the presence of iron oxides

random orientation of grains (Fig. 1a), which is usual in NC metals obtained by mechanical milling [18, 44, 45]. Figure 1b shows TEM micrograph of specimen obtained at 460 °C with grain size of ~46 nm. Increasing the temperature of consolidation makes it easier to identify the grain boundaries due to the reduction of overlapping. The average grain size of samples consolidated at 500 °C corresponds to low ultrafine-grained regime (~115 nm) moving away from the NC regime obtained with the lowest temperature (Fig. 1c). There is a visible weak ring inside the first ring of Fe{110}. The value of interplanar spacing associated to that ring agrees well with the highest intensities of $FeCr_2O_4$ and Fe_3O_4.

When the consolidated specimens at 500 °C are heat treated, larger ferrite and cementite precipitates are observed. Samples heat treated at temperatures up to 725 °C, show growth of ferritic grain up to 400 nm and small cementite precipitates (Fig. 1d). With treatment temperatures higher than 725 °C the grain size is significantly increased (Fig. 1e, f). The growth of ferrite grains is pinned by the presence of finely dispersed cementite and oxides along grain boundaries. Their presence is also detected in the XRD profiles (Fig. 2). At the consolidation temperatures used in this work, Zhang et al. [33] suggest that C atoms are mainly segregated at the grain boundaries of the nanocrystalline ferrite forming non-stoichiometric cementite particles, although there are important concentrations of C atoms inside the ferrite grains. Ohsaki et al. pointed out the large variations of carbon concentration in nanocrystalline ferrite (0.6–1.5 at.%). Some grains show concentrations up to 1.0 at.%, which is much larger than the equilibrium solubility of carbon in ferrite [46]. Regarding the O atoms, they are dissolved after long mechanical milling times [22, 27]. With annealing, the nano-sized oxide particles are finely dispersed within the ferrite matrix. The three-dimensional atom probe (3DAP) analysis by Srinivasarao et al. [35] has shown that O and Cr in mechanical milling of iron form oxide particles specially Fe_3O_4 and $FeCr_2O_4$. The examination of these oxides in the ferrite matrix by TEM dark-field images showed a regular distribution in grain boundaries and a very small size generally below 20 nm. High-temperature annealing above 700 °C are needed for precipitation of large oxides on the ferrite grain boundaries. The uniform distribution of these oxide particles controls the microstructure evolution inhibiting the accelerated growth of the grain during heat treatment [28]. Microstructure evolution details can be founded in previous works [47].

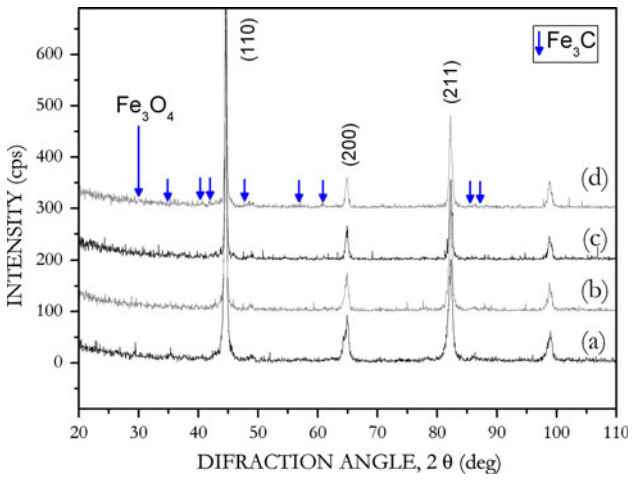

Fig. 2 XRD profile for different consolidation procedure. (*a*) HC 460 °C, (*b*) HC 500 °C, (*c*) HC 500 °C + HT 725 °C, (*d*) HC 500 °C + HT 775 °C

Figure 3 shows SEM images of porosity at internal section of specimens for three different conditions of consolidation. Samples consolidated at 425 °C show the highest total area of pores ~2.15% (Fig. 3a). The average size of pores is kept in the nanometric regime with a few pores around ~300 nm. This porosity decreases to 1.38% in samples consolidated at 500 °C (Fig. 3b). Samples with heat treatment show a little reduction of porosity as can be seen in Fig. 3c. Porosity analysis shows a low quantity of pores with small dimensions and homogenously distributed, which are the properties belonging to a closed porosity. The pores shape is very regular with shape factor around 0.9. These results suggest that total porosity is reduced when consolidation temperature increases, as well as remaining pores become more regular.

Compression test

Figure 4 shows stress–strain curves of compression tests at room temperature for samples with a wide range of grain sizes. As a general rule, the compressive strength decreased as the grain size increased. In samples with the smallest grain sizes, high compressive strength accompanied by a fragile behavior was noticed. Once in the UFG range, as the grain size was increased, the strength was decreased and the ductility was improved. The samples in the NC range had high strength but were fragile. Although the samples showed compressive strength over 2300 MPa, which represents an increase of nearly five times comparing with a conventional steel of the same carbon content, the samples failed before show plastic deformation. The analysis of the fracture surface showed that the fragile fracture initiated between powder particles (Fig. 5). This fact is related to a weak interparticle bonding, probably produced by the low consolidation temperature. Low ultrafine-grained samples (115 and 160 nm) showed small ductility. The strength reached is significantly lower than for the NC steels. For instance, samples with grain size of ~160 nm failed at ~1800 MPa and 2% of total deformation.

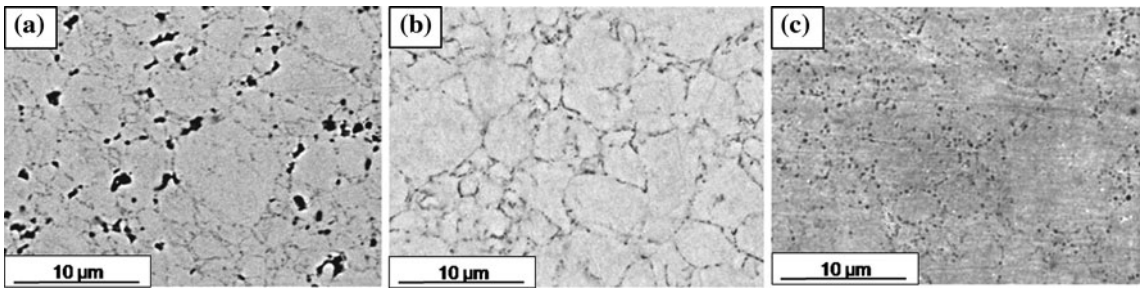

Fig. 3 SEM images of porosity for three different conditions of consolidation. **a** HC 425 °C, **b** HC 500 °C, **c** HC 500 °C + HT 725 °C

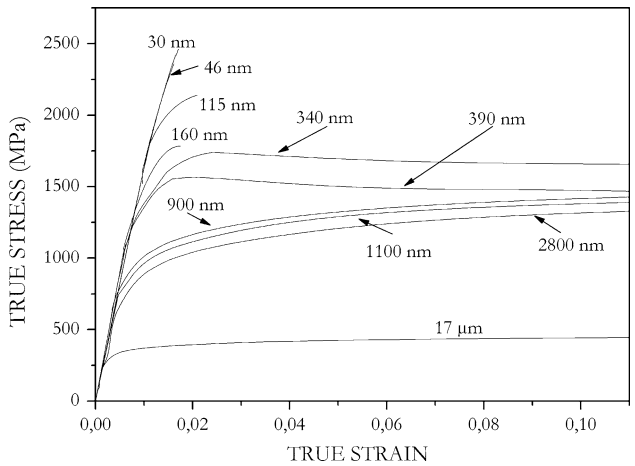

Fig. 4 Compression stress–strain curves of NC/UFG steel (0.55 wt% C) with several average grain size

The medium ultra-fine grained samples (340 and 390 nm) showed enhanced ductility and a significant reduction of compressive strength comparing with NC samples. It is worth noting that these samples showed more than 80% of plastic deformation (at this deformation value, the test was suspended), without showing defects that indicates the failure in the samples. In samples with an average grain size of 340 nm highlights yield point of 1335 MPa and an ultimate compressive strength of 1740 MPa at 2.4% total strain. From this point, softening appears until the end of the test. Same behavior was observed in samples with average grain size of 390 nm. Softening is not usual in polycrystalline metals, which usually show hardening during plastic deformation [9]. This absence of strain hardening has been analyzed in several works on samples of BCC metals, such as iron [10–12, 15], vanadium, and tantalum [48].

Slight ductility and strain-hardening capability due to the existence of localized deformation in shear bands has been studied in several works [10–15]. However, in the samples analyzed in this work, no shear bands have been detected. Other possible explanation is dynamic recovery, in which the steady state dislocation density is determined by the dynamic balance between the generation of dislocations during plastic deformation and annihilation during the recovery process [14]. This dynamic recovery can be promoted through a combination of very small grain size $<$400 nm and high stress applied. In this case, the sources of the dislocations are very close promoting a high frequency of annihilation.

The ultrahigh-grain samples (900 nm) show yield strength of 960 MPa, with an ultimate strength of 1490 MPa. Additionally, samples with grain size exceeding the UFG regime, reaching an average grain size of

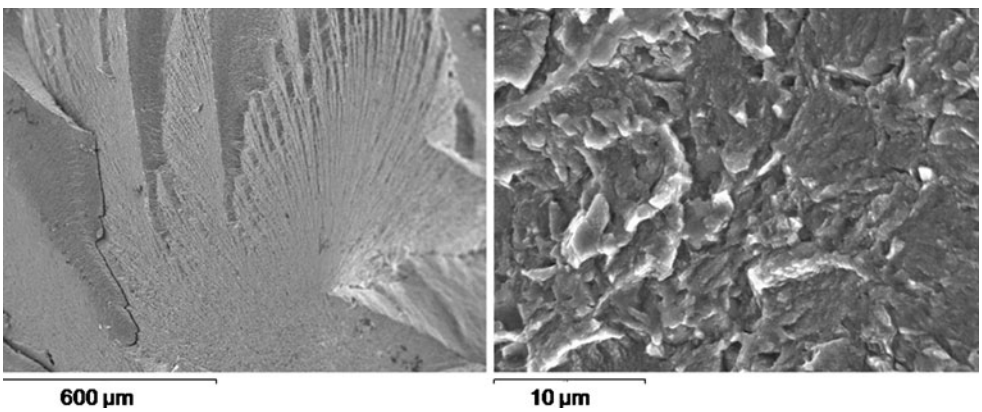

Fig. 5 Fragile fracture by compression test of NC samples with average grain size of 46 nm

1100 and 2800 nm show yield strength of 880 and 770 MPa, respectively. These samples show a plastic deformation above 80% (at this deformation value, the test was discontinued) with a yield point nearly twice to steels with conventional grain size (17 μm). The samples with grain size of 900, 1100, and 2800 nm show great strain-hardening capability developing an ultimate strength after a plastic deformation upper to 30%. This increase in the strain-hardening capability can be explained by a combination of different causes related to heat treatment >775 °C subsequently to the consolidation process. First, the presence of soft and ductile ferrite due to the carbon atom diffusion during the heat treatment, second, growth of ferrite grains which could reduce the excessive annihilation of dislocations during recovery processes, and finally, better metallurgical bonding due to the subsequent thermal treatment.

Mechanical properties under the compression mode for NC/UFG grained ferrite materials differ according to the manufacturing method used. Bulk NC Fe materials produced by cold compaction and hot pressing have a very high yield strength of ~2500 MPa but a very low plastic strain of less than 5% [10, 13]. Ma et al. pointed out the reason for the low plastic strain is the inability of dislocation activities in the nanocrystalline microstructure. Nearly fully dense compacts were produced by hot isostatic pressing at ~600 °C after mechanical milling [49]. However, they showed little plastic strains in compression due to shear banding as dominant deformation mechanism, even though the strength level was ~1800 MPa.

On the other hand, samples obtained by spark plasma sintering [33–35, 50] show an improvement of ductility with low reduction of strength. The yield strength of ~1800 MPa and compressive plastic strain reaches ~37% obtained in samples at 600 °C for 10 min is a good example of suitable relation strength/strain. However a limitation of spark plasma sintering technique refers to very small samples dimensions obtained (2 × 4 mm) compared to the samples in this work. In spite of these differences, the strength values of this work are very high, only surpassed by specimens reported by Srinivasarao et al. [50].

Tensile test

The tensile stress–strain curves for samples with average grain sizes from 46 nm to 1.7 μm are exposed in Fig. 6. As expected, the tensile strength decreased as the grain size increased. At the same time, there was an increase of ductility as the grain size increased. In the NC range, the behavior was clearly brittle, since all samples presented early failure in elastic regime, for such reason the curves for NC samples are not shown in Fig. 6. The fracture surface of ~46 nm specimen (Fig. 7a) shows particle debonding as the dominating fracture process, indicating a weak cohesion between former powder particles. This weak interparticle bonding is related mainly to the low temperature in the consolidation step.

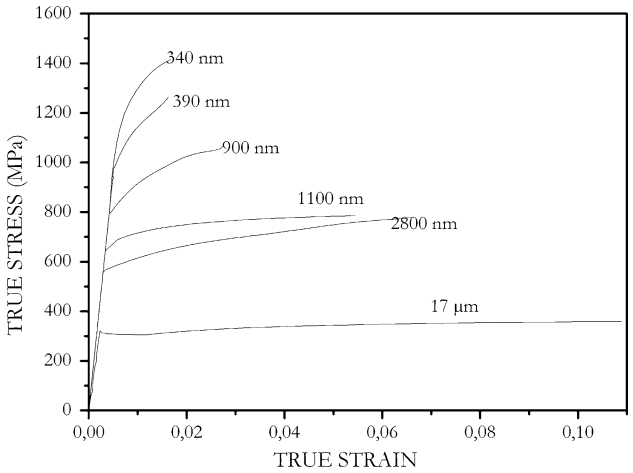

Fig. 6 Tensile stress–strain curves of NC/UFG steel (0.55 wt% C) with several average grain size

In the medium UFG range, there was an improvement of the bonding between powder particles, since the yield strength was 1240 and 1070 MPa for the specimens with average grain sizes of 340 and 390 nm, respectively. However, the samples were no ductile, with total strain below ~2%. Despite the increase in heat treatment temperature for these samples, the aspect of the fracture is clearly brittle (Fig. 7b). For the samples on the high UFG range, a slight improvement of ductility has been obtained as the heat treatment temperature was increased. At the same time, the strength values are reasonable, especially for samples with 900 nm average grain size, in which the yield strength rose above 840 MPa. The fracture surface for the specimens' heat treated at 825 °C with 1100 nm average grain size in Fig. 7c showed no signs of cleavage or interparticle debonding, but numerous zones with microdimples confirming the existence of plastic strain. Although the initiation point of the fracture is not clearly observed, it is likely that fracture initiates with the nucleation of a crack from larger and irregular pores where there is greater effect of stress concentration. In all cases, the stress–strain curves showed strain hardening, with no signs of lower and upper yield stress. The latter agrees well with the experimental fact that no shear bands have been observed in any sample. Finally, Fig. 6 shows tensile curve of samples with a ferritic grain size around 17 μm, offering yield strength of 357 MPa and ductility greater than all samples analyzed above. These behaviors support, as expected, that increase of heat treatment allows improvement of cohesion between particles.

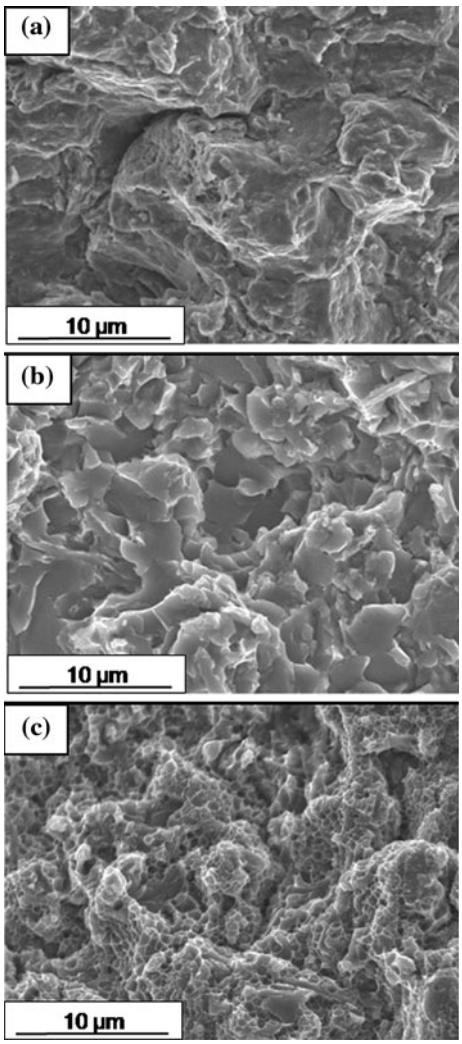

Fig. 7 Surface fracture of samples with average grain size of **a** 46 nm, **b** 340 nm, **c** 1100 nm

Tensile curves show little deformation capability reaching quickly the ultimate strength at very low deformation. Additionally, the subsequent heat treatment produces a slight increase of ductility, especially for a large grain size as 2.8 μm. This behavior can be related to two main facts. First, closed porosity, i.e., pores in small amounts, small size and homogenously distributed which reduce the deformation capacity. Probably the great amount of micro-porosity generates that several cracks initiate in different points and propagate until converging and forming a macro-crack. This macro-crack finally raises an unexpected failure. In fact, an important amount of micro-cracks has been observed in adjacent zones to the final failure supporting this idea. The results obtained suggest that the presented porosity is invariable when temperature treatment is increased; therefore the plastic deformation is almost constant. Shear bands and Lüders bands were not observed in any tested specimen. This fact could be also attributed to porosity, which generates stress concentrators avoiding any possibility of bands generation. According to Wang and Ma [14], in tensile tests, samples develop quickly the fracture by localized deformation in the neck, inhibiting the formation of shear bands.

Tejedor et al. [51] point out that carbon atoms inside ferrite grains and in the core of dislocations difficult the movement of dislocations reducing the plastic deformation. The slight improvement of strain-hardening capability observed in samples with heat treated higher than 800 °C, suggests better mobility of dislocations inside ferrite grains due to carbon diffusion and growth of ferritic grains. The fracture surface (Fig. 7c) showed many zones with microdimples that confirmed the improvement of ductility. This improved strain-hardening capability due to heat treatment was also observed by Song et al. [52] in UFG steel with a fine particle distribution of cementite. Additionally, the presence of hard second phases from Cr and O elements is related to the diminution of Lüders band formation and decrease of work-hardening in tensile samples of ferrite samples [53]. Therefore, it is possible that the combination of C element and hard second phases could restrict the mobility of dislocations in the coarse grains.

Tensile strength values obtained in this investigation are not directly comparable to other references due to differences in processing methods and testing conditions. Most of UFG microstructures have been produced by severe plastic deformation methods and advanced thermomechanical routes. UFG steel obtained by ECAP technique [38, 39] and ARB technique [40–43] show an improvement of ductility compared to the results of this work, probably due to lack of porosity. Ohmori et al. [40], and Torizuka et al. [41] work with Fe–C alloys (0.3–0.45% C). They observed yield strength of ~900 MPa, smaller than values reported in this investigation due to large grain size and minor carbon quantity. Nevertheless, their samples show a high ductility of 18%, several times higher than ductility reported in this paper. Also, Liu et al. and Zhao et al. observed ductility values higher than those reported here [42, 43]. Zhao et al. worked with a carbon amount equivalent to the steel of this investigation, but their steel has conventional quantity of Mn and Si elements. Yield strength of ~1000 MPa can be explained as the effect of the combination of such elements, as well as they reported a ductility of ~16% pointing out the advantages of ARB technique compared to the powder consolidation process used in this research [43]. Besides, Shin et al. [39] pointed out a good relation strength/strain with yield strength slight lower than our results and ductility of 11%.

Cheng et al. [54] reported tensile behavior of submicrometer iron samples obtained by mechanical milling and consolidate by rapid forging method. They reported a yield strength of ~900 MPa in samples with a grain size of

1.6 μm. The low ductility ~3% indicates the significant effect of lack of bonding between particles by rapid forging method. Takaki et al. [23] obtained NC iron powder by means of mechanical milling and subsequently accumulative rolling between 600 and 800 °C. They reported yield strength of ~1800 MPa with grain size of ~180 nm, being a little inferior to yield strength obtained in this investigation. Also, the low ductility of 2% reported by Takaki et al. can be a consequence of the porosity of the material, as it happened in this investigation.

The influence of specimens' dimensions and strain measurement methods may cause serious differences in the reported results. Recently, Zhao et al. studied the size effect on ductility and especially the uniform elongation in small copper specimens. Although nanostructured materials processed by SPD were not tested because of their small uniform elongations being difficult to evaluate the size effect. FEM simulation and earlier work on nanostructured Cu and NiFe alloy showed a trend whereby the uniform elongation increase with decreasing gauge length and increasing specimen thickness when strain was measured from the crosshead displacement, such as measured in this investigation [55, 56].

Tensile test results are noticeably different to compression test results explained above. These differences can be explained by two main reasons: first, geometric differences between the cylindrical test samples of compression (7 × 5 mm) and the tensile test samples obtained from disks (1 × 9.2 mm) generate different conditions of friction during uniaxial consolidation process. Finally, tensile tests are high sensitive to porosities of the material, that is why the compression tests are much more permissive [33]. Figure 8 shows two specimens with clear differences between compression and tensile behavior. Medium ultrafine samples (340 nm) display compression strength appreciably higher than tensile tests results. Both curves show a lack strain-hardening capability reaching ~2.4% in compression and 1.6% in tensile of plastic deformation. The curves behavior is different when strain-hardening capability is used up. High ultrafine-grained samples (900 nm) display compression strength higher than tensile tests, like happened in the case of medium ultrafine samples. As explained above, porosity contained in tensile test samples creates and propagates cracks before these samples saturate their strain-hardening capability.

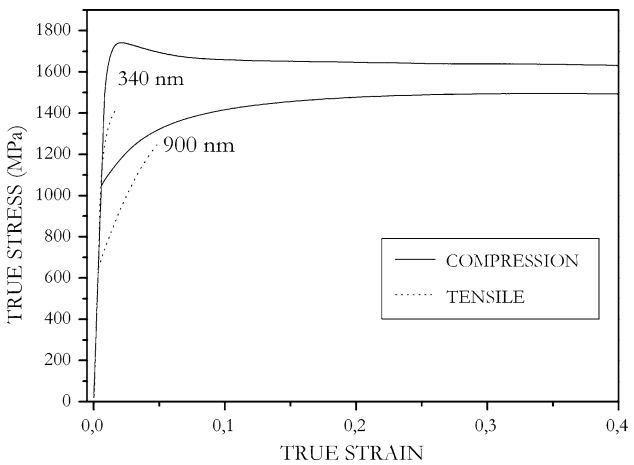

Fig. 8 Compression and tension stress–strain curves for samples with grain size of 340 and 900 nm

Conclusions

The mechanical milling, hot compaction process, and subsequent heat treatments have enabled the production of bulk samples of 0.55 wt% C steel with ferritic grain size into the nanocrystalline and ultrafine regimens. The growth of ferrite grains is pinned by the presence of finely-dispersed cementite and oxides in grain boundaries.

As a general rule, the compressive and tensile strength decreased as the grain size increased. Samples with smaller grain sizes show a high strength accompanied by a fragile behavior. Once in the UFG range, as the grain size was increased, the strength was decreased and the ductility was improved. Tensile test results are noticeably different to compression test results. These differences can be explained by geometric differences between compression and tensile test samples. Additionally, tensile tests are highly sensitive to the porosity of the material where the compression tests are much more permissive.

Tensile curves show little deformation capability reaching quickly the ultimate strength at very low deformation. Shear and Lüders bands were not observed in any specimen tested. This fact could be attributed firstly to the porosity, the presence of second phases from Cr and O elements, and carbon atoms inside of ferrite grains and in the core of dislocations. They could restrict the mobility of dislocations reducing the plastic deformation.

Acknowledgements The authors wish to thank R. Tejedor for his support in the discussion results and M. Marsal for their assistance in SEM observations. This work was supported by the Spanish CICYT (project DPI 2005-09324) and Universidad Nacional de Colombia.

References

1. Song R, Ponge D, Raabe D, Speer JG, Matlock DK (2006) Mater Sci Eng A 441:1
2. Liu ZG, Fecht HJ, Umemoto M (2004) Mater Sci Eng A 375–377:839
3. Han BQ, Yue S (2003) J Mater Proc Technol 136:100
4. Wang YM, Chen M, Zhou F, Ma E (2002) Nature 419:912

5. Han BQ, Lavernia EJ, Mohamed FA (2005) Rev Adv Mater Sci 9:1
6. Lesuer DR, Syn CK, Sherby OD (2005) Mater Sci Eng A 410–411:222
7. Zhao YH, Liao XZ, Cheng S, Ma E, Zhu YT (2006) Adv Mater 18:2280
8. Zhao MC, Nahamura T, Qiu H, Nagai K, Yang K (2006) Scripta Mater 54:1193
9. Dieter GE (1988) Mechanical metallurgy SI metric. McGraw-Hill, London, UK
10. Carsley JE, Fisher A, Milligan WW, Aifantis EC (1998) Metall Mater Trans A 29A:2261
11. Jia D, Ramesh KT, Ma E (2000) Scripta Mater 42:73
12. Jia D, Ramesh KT, Ma E (2003) Acta Mater 51:3495
13. Ma E (2003) Scripta Mater 49:663
14. Wang YM, Ma E (2004) Mater Sci Eng A 375–377:46
15. Wei Q, Kecskes L, Jiao T, Hartwig KT, Ramesh KT, Ma E (2004) Acta Mater 52:1859
16. Kimura Y, Takaki S (1995) Mater Trans 36(2):289
17. Yin J, Umemoto M, Liu ZG, Tsuchiya K (2001) ISIJ Int 41:1389
18. Malow TR, Koch CC (1998) Metall Mater Trans A 9A:2285
19. Xu Y, Umemoto M, Tsuchiya K (2002) Mater Trans 43:2205
20. Sakai Y, Ohtaguchi M, Kimura Y (2000) In: Symposium on ultrafine grained materials at the 2000 TMS Annual Meeting, p 361
21. Belyakov A, Sakai Y, Hara T, Kimura Y, Tsuzaki K (2001) Scripta Mater 45:1213
22. Belyakov A, Sakai Y, Hara T, Kimura Y, Tsuzaki K (2003) Scripta Mater 48:1111
23. Takaki S, Kawasaki K, Kimura Y (2001) J Mater Proc Technol 117:359
24. Khan AS, Zhang H, Takacs L (2000) Int J Plast 16:1459
25. Lillo T, Korth G (1998) Nanostruct Mater 10:95
26. Livne Z, Munitz A, Rawers JC, Fields RJ (1998) Nanostruct Mater 10:503
27. Lesuer DR, Syn CK, Sherby OD (2006) Mater Trans 47(6):1508
28. Kimura Y, Kawasaki K, Goto HY, Takaki S (2000) In: Symposium on ultrafine grained materials at the 2000 TMS Annual Meeting
29. Belyakov A, Sakai Y, Hara T, Kimura Y, Tsuzaki K (2004) Mater Trans 45(7):2252
30. Korznikov AV, Ivanisenko YV, Safarov LM, Valiev RZ (1994) Nanostruct Mater 4(2):159
31. Todaka Y, Umemoto M, Yin J, Liu Z, Tsuchiya K (2007) Mater Sci Eng A 462:264
32. Umemoto M (2003) Mater Trans 44(10):1900
33. Zhang HW, Gopalan R, Mukai T, Hono K (2005) Scripta Mater 53:863
34. Oh-ishi K, Zhang HW, Ohkubo T, Hono K (2007) Mater Sci Eng A 456:20
35. Srinivasarao B, Oh-ishi K, Ohkubo T, Hono K (2008) Scripta Mater 58:759
36. Malow TR, Koch CC (1997) Acta Mater 45(5):2177
37. Rawers J (1999) Nanostruct Mater 11:1055
38. Park KT, Kim YS, Lee JG, Shin DH (2000) Mater Sci Eng A 293:165
39. Shin DH, Park KT (2005) Mater Sci Eng A 410–411:299
40. Ohmori A, Torizuka S, Nagai K (2004) ISIJ Int 44(6):1063
41. Torizuka S, Muramatsu E, Murty NS, Nagai K (2006) Scripta Mater 55:751
42. Liu MY, Shi B, Wang C, Ji SK, Cai X, Song HW (2003) Mater Lett 57:2798
43. Zhao M, Hanamura T, Qiu H, Nagai K, Yang K (2006) Scripta Mater 54:1385
44. Kimura Y, Kawasaki K, Futamura Y, Takaki S (2006) Mater Sci Forum 503–504:317
45. Liu ZG, Fecht HJ, Xu Y, Yin J, Tsuchiya K, Umemoto M (2003) Mater Sci Eng A 362:322
46. Ohsaki S, Hono K, Hidaka H, Takaki S (2005) Scripta Mater 52:271
47. Rodriguez Baracaldo R, Benito JA, Cabrera JM, Prado JM (2008) Mater Sci Eng A 493:215
48. Wei Q, Cheng S, Ramesh KT, Ma E (2004) Mater Sci Eng A 381:71
49. Munitz A, Livne Z, Rawers JC, Adams JS, Fields RJ (1999) Nanostruct Mater 11:159
50. Srinivasarao B, Oh-ishi K, Ohkubo T, Hono K (2009) Acta Mater 57:3277
51. Tejedor R, Rodriguez Baracaldo R, Benito JA, Cabrera JM (2008) Scripta Mater 59:631
52. Song R, Ponge D, Raabe D (2005) Scripta Mater 52:1075
53. Tomota Y, Narui A, Tsuchida N (2008) ISIJ Int 48:1107
54. Cheng S, Milligan WW, Wang X, Choo H, Liaw PK (2008) Mater Sci Eng A 493:226
55. Wei H, Hibbard GD, Palumbo G, Erb U (2007) Scripta Mater 57:996
56. Zhao YH, Guo YZ, Wei Q, Topping TD, Dangelewicz AM, Zhu YT, Langdon TG, Lavernia EJ (2009) Mater Sci Eng A 525:68